

# $\mu$ Bi-ConvLSTM: An Ultra-Lightweight Efficient Model for Human Activity Recognition on Resource Constrained Devices

Mridankan Mandal

Department of Information Technology  
 Indian Institute of Information Technology, Allahabad  
 Prayagraj, India  
 mridankanmandal2006@gmail.com

**Abstract**—Human Activity Recognition (HAR) on resource-constrained wearables requires models that balance accuracy against strict memory and computational budgets. State of the art lightweight architectures such as TinierHAR (34K parameters) and TinyHAR (55K parameters) achieve strong accuracy, but exceed memory budgets of microcontrollers with limited SRAM once operating system overhead is considered.

We present  $\mu$ Bi-ConvLSTM, an ultra-lightweight convolutional recurrent architecture achieving 11.4K parameters on average through two-stage convolutional feature extraction with  $4\times$  temporal pooling and a single bidirectional LSTM layer. This represents  $2.9\times$  parameter reduction versus TinierHAR and  $11.9\times$  versus DeepConvLSTM while preserving linear  $O(N)$  complexity.

Evaluation across eight diverse HAR benchmarks shows that  $\mu$ Bi-ConvLSTM maintains competitive performance within the ultra-lightweight regime: 93.41% macro F1 on UCI-HAR, 94.46% on SKODA assembly gestures, and 88.98% on Daphnet gait freeze detection. Systematic ablation reveals task dependent component contributions where bidirectionality benefits episodic event detection, but provides marginal gains on periodic locomotion. INT8 post training quantization incurs only 0.21% average F1-score degradation, yielding a 23.0 KB average deployment footprint suitable for memory constrained edge devices.

**Index Terms**—Edge AI, Human Activity Recognition, Lightweight Neural Networks, Convolutional LSTM, Ubiquitous computing, Bidirectional LSTM, TinyML, Parameter Efficiency

## I. INTRODUCTION

Human Activity Recognition (HAR) from wearable inertial sensors enables critical applications across healthcare, fitness, and ubiquitous computing [6], [9]. Continuous freeze of gait detection for Parkinson’s disease patients [15], real time fall detection for elderly care [17], and always on fitness tracking [10] share a common requirement of deployment on resource constrained wearable devices where battery life and form factor are important.

Deep learning has substantially improved HAR accuracy through hierarchical temporal pattern learning [1], [5]. However, an inherent trade-off exists between model capacity and deployment feasibility. DeepConvLSTM [1], the canonical convolutional recurrent architecture, achieves strong accuracy, but requires 136K parameters and 15.5M MACs, rendering it impractical for microcontroller based wearables. Recent

lightweight alternatives partially address this gap: TinyHAR [2] reduces to 55K parameters using cross channel attention, but introduces  $O(N^2)$  sequence complexity, and TinierHAR [3] achieves 34K parameters through depthwise separable convolutions and bidirectional GRUs, representing the current state of the art in lightweight HAR.

Yet a deployment gap remains. Microcontrollers with very limited on-chip SRAM must also reserve memory for the operating system, sensor drivers, and communication stacks, leaving only a small fraction for neural network weights and intermediate activations. In practice, even models as compact as TinierHAR can exceed this usable budget once activation memory during inference is considered. This motivates architectures that push parameter counts much lower while still preserving strong temporal modeling capacity.

We introduce  $\mu$ Bi-ConvLSTM, engineered to maximize information density within an ultra-constrained parameter budget. Our contributions:

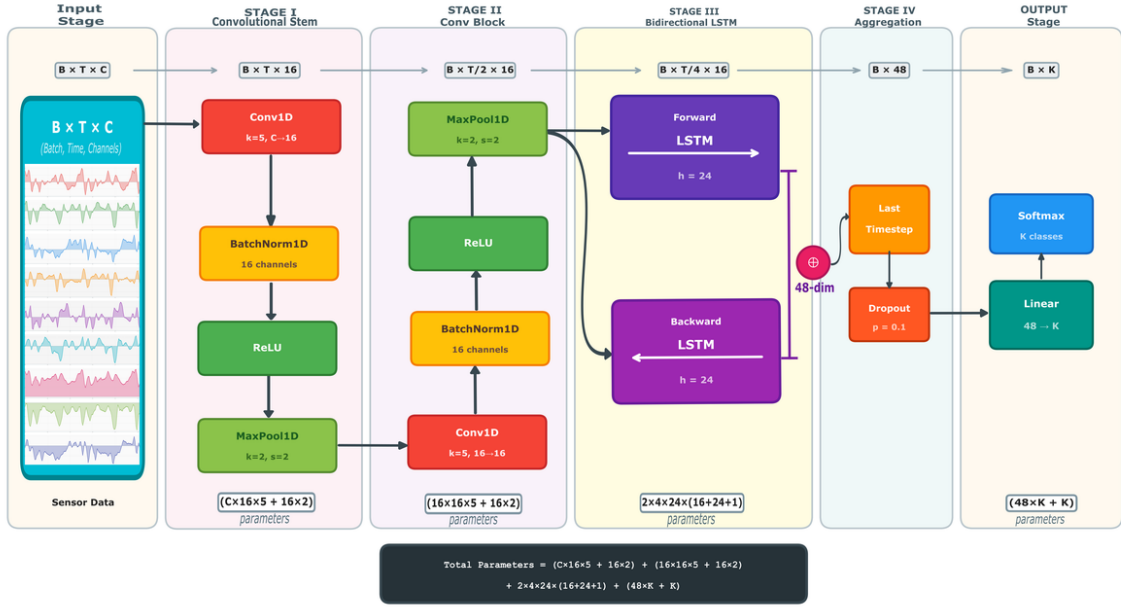
- An 11.4K parameter architecture (averaged across datasets) achieving  $2.9\times$  reduction versus TinierHAR through a two stage convolutional stem with  $4\times$  temporal pooling and single layer bidirectional LSTM, maintaining strict  $O(N)$  complexity.
- Comprehensive evaluation across eight diverse HAR benchmarks demonstrating competitive accuracy within the ultra-lightweight regime, with performance gaps systematically characterized against dataset complexity.
- Systematic ablation studies revealing task dependent component contributions: bidirectionality proves essential for episodic events, but optional for periodic activities.
- Quantization analysis showing 0.21% average INT8 degradation within a 23.0 KB average deployment footprint suitable for memory constrained devices.

Figure 1 illustrates the architecture. The design achieves 11.4K parameters on average with strict  $O(N)$  complexity, enabling deployment within memory constrained environments.

## II. RELATED WORK

We review HAR architectures along the accuracy-efficiency spectrum, positioning  $\mu$ Bi-ConvLSTM within the ultra-

## Micro-Bi-ConvLSTM Architecture



**Fig. 1:**  $\mu$ Bi-ConvLSTM architecture overview. Input sensor signals ( $C$  channels  $\times$   $T$  timesteps) pass through two convolutional blocks with batch normalization, ReLU activation, and  $2 \times$  max pooling each, achieving  $4 \times$  total temporal compression. A single bidirectional LSTM (hidden dimension 24) processes the compressed sequence, with the final timestep representation feeding the classification head. Parameter count varies with input channels and output classes.

lightweight regime.

### A. Deep Learning Architectures for HAR

DeepConvLSTM [1] established the convolutional recurrent paradigm: four convolutional layers (64 filters each) followed by two stacked LSTMs, totaling 136K parameters. While achieving strong accuracy, this architecture proves unsuitable for microcontroller deployment. Subsequent work explored ensemble approaches [4] and multi-modal fusion [7], further increasing computational requirements.

Attention based approaches demonstrate superior long range dependency modeling. Abedin et al. [33] achieve SOTA performance through attend and discriminate mechanisms, while GlobalFusion [34] and AttnSense [35] leverage multi-level attention for sensor fusion. However, these methods require  $>100$ K parameters, exceeding edge deployment budgets.

### B. Lightweight HAR Architectures

Recognizing deployment constraints, recent work explores model compression:

**Efficient Convolutions:** TinierHAR [3] achieves 34K parameters through depthwise separable convolutions and bidirectional GRUs, representing current SOTA efficiency. MLP-HAR [37] uses purely fully connected layers with FFT pre-processing, achieving 55K parameters, but requiring spectral transformation.

**Attention-based Compression:** TinyHAR [2] reduces to 55K parameters using cross channel attention, but introduces

$O(N^2)$  sequence complexity. Murahari and Plötz [36] analyze attention mechanisms for HAR, finding diminishing returns on shorter sequences typical of wearable data.

**Knowledge Distillation:** Deng et al. [38] transfer knowledge from large teachers to compact students, achieving competitive performance with 50% parameter reduction, but still exceeding microcontroller budgets.

### C. Transformers versus Recurrent Architectures

The success of Transformers in NLP [41] has motivated their application to HAR. However, recent studies reveal important trade-offs for wearable deployment. Lattanzi et al. [42] systematically evaluate Transformers on tiny devices, finding that while attention mechanisms excel at capturing long range dependencies, their quadratic complexity and memory requirements often exceed microcontroller budgets. Murahari and Plötz [36] demonstrate diminishing returns of attention on shorter sequences typical of HAR (128-256 timesteps), where local temporal patterns dominate. Bock et al. [43] show that shallow LSTMs can match deeper architectures on HAR tasks, suggesting that inductive biases of recurrent models align well with the sequential nature of human motion. These findings motivate our choice of BiLSTM over attention based alternatives.

### D. Model Compression Techniques

Post-training quantization [27], [28] enables INT8 deployment with minimal accuracy loss. Yi et al. [39] combine prun-

**TABLE I:** Architectural Comparison of HAR Models

Model	Conv Type	Temporal	Attention	Params	Complexity
DeepConvLSTM	Standard	2×LSTM	No	136K	$O(N)$
TinyHAR	Standard	LSTM+Attn	Yes	55K	$O(N^2)$
TinierHAR	Depthwise	BiGRU+Attn	Yes	34K	$O(N^2)$
$\mu$ Bi-ConvLSTM	Standard	BiLSTM	No	<b>11.4K</b>	$O(N)$

ing and quantization for wearable HAR, achieving reduced footprints while maintaining accuracy. Neural Architecture Search [40] automates architecture exploration, but requires extensive computational resources.

#### E. Positioning of $\mu$ Bi-ConvLSTM

Despite these advances, a gap persists for sub-15K parameter models compatible with the most constrained microcontrollers. Table I compares architectural choices.  $\mu$ Bi-ConvLSTM adheres to the proven convolutional recurrent paradigm while achieving 4× temporal compression through pooling, substantially reducing LSTM sequence length. Unlike attention based approaches including Transformers, strict  $O(N)$  complexity is maintained, with the recurrent inductive bias that aligns with sequential motion data. Unlike depthwise separable convolutions, standard convolutions preserve cross channel information flow critical for low dimensional sensor data (3-9 channels typical in smartphone HAR).

### III. METHODOLOGY

#### A. Design Principles

Based on analysis of HAR data characteristics and edge deployment constraints, we developed the following design principles:

**P1: Aggressive Temporal Reduction.** Unlike image data with comparable spatial dimensions, HAR exhibits extreme aspect ratios ( $T=128\text{-}256$  timesteps,  $C=3\text{-}9$  channels). Long sequences pose challenges for recurrent models because memory scales linearly with sequence length, and gradient propagation degrades over extended horizons. Temporal pooling reduces computational cost while preserving salient motion patterns.

**P2: Standard Convolutions for Low Dimensional Input.** For sensor data with few channels (3-9 typical), standard convolutions provide superior cross channel feature extraction versus depthwise separable variants. Depthwise operations limit cross channel information flow, critical when accelerometer and gyroscope channels contain complementary motion cues.

**P3: Single Wide Recurrent Layer.** Given parameter constraints, we allocate capacity to a single wide BiLSTM ( $H=24$ ) rather than stacked narrow layers. This maximizes temporal modeling capacity while avoiding redundant hierarchical processing.

**P4: Bidirectional Processing.** Activities like freeze of gait show temporal asymmetry where onset differs from recovery. Bidirectional LSTMs capture both forward progression and backward context, though ablation studies (Section VI-A) reveal this benefit is task dependent.

**P5: Linear Complexity.** Real time applications require predictable inference time. We maintain strict  $O(N)$  complexity, avoiding attention mechanisms that introduce quadratic scaling.

#### B. Architecture Overview

$\mu$ Bi-ConvLSTM comprises five stages optimized for minimal overhead while preserving representational capacity, as illustrated in Figure 1.

#### C. Convolutional Stages

The input  $\mathbf{X} \in \mathbb{R}^{B \times T \times C}$  (batch size  $B$ , sequence length  $T$ , channels  $C$ ) undergoes two convolutional blocks extracting local temporal features:

$$\mathbf{H}_1 = \text{ReLU}(\text{BN}(\mathbf{W}_1 * \mathbf{X} + \mathbf{b}_1)) \quad (1)$$

where  $\mathbf{W}_1 \in \mathbb{R}^{F \times C \times K}$  with  $F = 16$  filters and kernel size  $K = 5$ . Max pooling after each block provides 2× temporal compression, yielding total 4× reduction:  $T \rightarrow T/4$ . The receptive field spans 9 timesteps, which is sufficient for activity relevant patterns like gait cycles and gesture transitions, computed as  $R = 1 + \sum_{i=1}^L (K_i - 1) \cdot \prod_{j=1}^{i-1} S_j$ .

#### D. Bidirectional LSTM

Compressed features pass through a single layer Bidirectional LSTM with hidden dimension  $H = 24$ :

$$\mathbf{i}_t = \sigma(\mathbf{W}_{ii}\mathbf{x}_t + \mathbf{W}_{hi}\mathbf{h}_{t-1} + \mathbf{b}_i) \quad (2)$$

$$\mathbf{f}_t = \sigma(\mathbf{W}_{if}\mathbf{x}_t + \mathbf{W}_{hf}\mathbf{h}_{t-1} + \mathbf{b}_f) \quad (3)$$

$$\mathbf{c}_t = \mathbf{f}_t \odot \mathbf{c}_{t-1} + \mathbf{i}_t \odot \tanh(\mathbf{W}_{ig}\mathbf{x}_t + \mathbf{W}_{hg}\mathbf{h}_{t-1}) \quad (4)$$

$$\mathbf{h}_t = \sigma(\mathbf{W}_{io}\mathbf{x}_t + \mathbf{W}_{ho}\mathbf{h}_{t-1} + \mathbf{b}_o) \odot \tanh(\mathbf{c}_t) \quad (5)$$

Bidirectional processing concatenates forward and backward passes into a 48 dimensional representation. We use last timestep aggregation:  $\mathbf{h}_{\text{agg}} = \mathbf{H}[:, -1, :]$ .

**Design Rationale:** BiLSTM was selected over alternatives for three reasons: (1) bidirectionality captures temporal asymmetry in episodic events where onset and recovery patterns differ; (2) LSTM’s separate cell state provides superior gradient flow versus GRU for longer compressed sequences ( $T/4 = 32$  timesteps); (3) last timestep aggregation avoids attention overhead while the final bidirectional state synthesizes both full forward sequence context and complete backward information.

#### E. Classification Head

The aggregated representation passes through dropout regularization and a linear classifier:

$$\hat{\mathbf{y}} = \text{Softmax}(\mathbf{W}_{\text{out}} \cdot \text{Dropout}(\mathbf{h}_{\text{agg}}) + \mathbf{b}_{\text{out}}) \quad (6)$$

**TABLE II:** Dataset Characteristics

Dataset	Type	Subjects	Classes	Channels	Frequency	Window
UCI-HAR [11]	Phone	30	6	9	50 Hz	128
MotionSense [12]	Phone	24	6	6	50 Hz	128
WISDM [10]	Phone	36	6	3	20 Hz	128
PAMAP2 [16]	Body IMU	9	12	19	100 Hz	128
Opportunity [13]	Body IMU	4	5	79	30 Hz	128
UniMiB [17]	Phone	30	9	3	50 Hz	128
SKODA [14]	Glove IMU	1	11	30	98 Hz	98
Daphnet [15]	Body IMU	10	2	9	64 Hz	64

### F. Parameter and Complexity Analysis

The architecture’s parameter count scales with input channels and output classes, ranging from approximately 10K to 32K across datasets (Table IV). The BiLSTM layer dominates at roughly 75% of total parameters, computed as  $P_{\text{LSTM}} = 2 \times 4 \times H \times (F + H + 1)$  where  $H$  is hidden size and  $F$  is input features. Total MACs scale linearly with sequence length  $T$  and input channels, with Table V showing 245K–1.14M MACs across configurations. This represents 32–42 $\times$  reduction versus DeepConvLSTM and 5–42 $\times$  versus TinyHAR, while maintaining strict  $O(N)$  complexity.

## IV. EXPERIMENTAL SETUP

### A. Datasets

Evaluation was done on eight publicly available HAR benchmarks spanning diverse sensing modalities, subject populations, and activity types (Table II). UCI-HAR [11] provides smartphone accelerometer and gyroscope data from 30 subjects performing six locomotion activities (walking, climbing stairs, sitting, standing, lying) at 50 Hz. MotionSense [12] similarly captures smartphone IMU data from 24 subjects, but includes device attitude information. WISDM [10] offers accelerometer only data from 36 subjects at lower 20 Hz sampling, testing model robustness to reduced input dimensionality.

PAMAP2 [16] and Opportunity [13] represent more challenging multi-sensor configurations. PAMAP2 fuses data from three body worn IMUs (19 channels) across 12 activities from 9 subjects, while Opportunity provides 79 channels from a dense sensor network with substantial class imbalance. UniMiB-SHAR [17] focuses on fall detection with 9 activity classes. SKODA [14] targets industrial assembly gesture recognition with 30 channel sensor gloves at 98 Hz from a single subject performing repetitive manufacturing tasks. Daphnet [15] addresses Parkinson’s disease gait freeze detection, a binary classification task with severe class imbalance (approximately 10% freeze events) requiring high sensitivity for clinical utility.

### B. Preprocessing and Signal Conditioning

Raw sensor signals undergo dataset specific preprocessing to address noise characteristics. For datasets with known high frequency noise (industrial and clinical settings), 4th order Butterworth low pass filtering was applied to: PAMAP2 (10 Hz cutoff), SKODA (5 Hz cutoff for motor vibration), and Daphnet (12 Hz cutoff). All features are z-score normalized

per channel using training set statistics. Sliding windows with 50% overlap generate samples.

For multi-subject datasets (UCI-HAR, MotionSense, WISDM, PAMAP2, UniMiB, Daphnet), subject wise cross validation splits were used, ensuring no data leakage between training and evaluation, that is, samples from the same subject never appear in both training and test sets. For single subject datasets (SKODA) and Opportunity with predefined protocol splits, the standard train/test partitions from the original publications were used. This subject independent evaluation protocol provides unbiased generalization estimates for deployment on unseen users.

### C. Training Protocol

All models train for a maximum of 200 epochs using AdamW [18] with cosine annealing learning rate scheduling. Early stopping with patience of 10 epochs was used, based on validation F1-score. For imbalanced datasets (Daphnet, Opportunity, PAMAP2), inverse frequency class weighting is applied in the cross-entropy loss.

Hyperparameter optimization (HPO) uses Optuna [19] with 50 Tree-structured Parzen Estimator (TPE) trials per dataset. Each HPO trial trains for 10 epochs with early stopping patience of 5 epochs to enable rapid exploration. The search space covers learning rate ( $10^{-4}$  to  $10^{-2}$ , log scale), weight decay ( $10^{-5}$  to  $5 \times 10^{-2}$ , log scale), and dropout (0.0 to 0.5, uniform). Architecture parameters remain frozen during HPO to isolate training dynamics from structural effects.

Final training uses the optimized hyperparameters for 200 epochs with early stopping patience of 10 epochs. We report macro F1-score mean and standard deviation across 5 random seeds generated from a master seed for reproducibility.

### D. Baseline Models

Comparison was made against three representative architectures spanning the efficiency spectrum, all trained with identical HPO and training protocols for fair comparison.

**DeepConvLSTM** [1] serves as the canonical high capacity baseline following the original specification: four convolutional layers with 64 filters each (kernel size 5, same padding), followed by two stacked unidirectional LSTM layers with 64 hidden units per layer. This configuration totals approximately 136K parameters.

**TinyHAR** [2] represents modern attention based lightweight design. The configuration from the original implementation was used: 24 filters across 4 convolutional layers with kernel size 5, and cross channel self attention for temporal fusion. This achieves approximately 55K parameters.

**TinierHAR** [3] provides the most aggressive prior compression using depthwise separable convolutions and bidirectional GRUs. The model is configured with 8 filters across 4 depthwise separable convolutional blocks with 16 GRU hidden units per direction, totaling approximately 34K parameters.

**TABLE III:** F1 Score Comparison (Macro %)

Dataset	$\mu$ Bi-ConvLSTM	DeepConvLSTM	TinyHAR	TinierHAR
UCI-HAR	93.41 $\pm$ 0.35	93.61 $\pm$ 0.56	96.53 $\pm$ 0.41	96.37 $\pm$ 0.59
MotionSense	91.65 $\pm$ 0.43	91.64 $\pm$ 0.75	92.67 $\pm$ 0.67	91.99 $\pm$ 0.60
WISDM	73.17 $\pm$ 12.4	81.25 $\pm$ 2.55	77.09 $\pm$ 4.95	83.06 $\pm$ 3.24
PAMAP2	60.75 $\pm$ 1.76	66.20 $\pm$ 2.72	73.22 $\pm$ 3.58	74.07 $\pm$ 1.16
Opportunity	87.58 $\pm$ 0.73	87.21 $\pm$ 0.63	88.69 $\pm$ 0.38	87.09 $\pm$ 0.90
UniMiB	79.43 $\pm$ 1.66	84.12 $\pm$ 2.23	77.61 $\pm$ 2.23	79.67 $\pm$ 4.45
SKODA	94.46 $\pm$ 1.31	95.25 $\pm$ 1.03	97.01 $\pm$ 0.53	96.99 $\pm$ 0.76
Daphnet	88.98 $\pm$ 1.64	88.19 $\pm$ 1.89	86.42 $\pm$ 3.64	89.84 $\pm$ 1.90
<b>Average</b>	83.68	85.93	86.16	<b>87.39</b>

## V. RESULTS

### A. Predictive Performance

Table III presents F1 scores across all benchmarks. Several patterns emerge from these results.

**Competitive Performance in Ultra-Lightweight Regime:** Despite  $2.9\times$  fewer parameters than TinierHAR,  $\mu$ Bi-ConvLSTM achieves comparable accuracy on smartphone IMU datasets. On UCI-HAR, the gap compared to TinyHAR (the best performer) is 3.12%, while on MotionSense the gap narrows to 1.02%.

**Strong Medical Monitoring Performance:** On Daphnet, gait freeze detection,  $\mu$ Bi-ConvLSTM achieves 88.98% F1, competitive with TinierHAR’s 89.84%. Both substantially outperform the attention based TinyHAR (86.42%), suggesting that recurrent architectures better capture the temporal dynamics of episodic freezing events than attention mechanisms for this binary classification task.

**Class Imbalance Sensitivity:** The performance gap between  $\mu$ Bi-ConvLSTM and larger baselines varies systematically with dataset characteristics. PAMAP2 shows a 13.3% F1-score gap as compared to TinierHAR due to extreme class imbalance where rare activities (rope jumping, cycling) constitute  $<10\%$  of samples. Ultra-lightweight models prioritize majority classes under capacity constraints, degrading macro F1-score. In contrast, Opportunity’s balanced gesture distribution enables competitive performance (87.58% vs. 87.09%) despite its 79 channel density, demonstrating that class distribution impacts lightweight models more than sensor dimensionality. The WISDM results show high variance (12.4% std), likely due to the dataset’s lower sampling rate (20 Hz) and minimal channel count (3) creating challenging optimization dynamics.

Figure 2 visualizes performance distributions. Despite  $2.9\times$  fewer parameters than TinierHAR,  $\mu$ Bi-ConvLSTM maintains competitive accuracy with tight variance on UCI-HAR and SKODA, both well structured datasets with clear activity boundaries.

### B. Computational Efficiency

Table IV quantifies efficiency advantages.  $\mu$ Bi-ConvLSTM achieves 7.34 F1 per thousand parameters and 172.5 F1 per million MACs. Compared to TinierHAR, this represents  $2.8\times$  and  $3.4\times$  improvements respectively. This efficiency stems from our architectural choices: temporal pooling reduces LSTM sequence length by  $4\times$ , and the single layer bidirectional design eliminates redundant stacked processing.

**TABLE IV:** Computational Efficiency Comparison

Metric	$\mu$ Bi-ConvLSTM	DeepConvLSTM	TinyHAR	TinierHAR
Parameters	<b>11.4K</b>	135.6K	55.1K	33.5K
MACs	<b>485K</b>	15.51M	9.29M	1.73M
F1/K-Params	<b>7.34</b>	0.63	1.56	2.61
F1/M-MACs	<b>172.5</b>	5.54	9.27	50.5
Complexity	$O(N)$	$O(N)$	$O(N^2)$	$O(N^2)$

**TABLE V:** MACs by Dataset (thousands)

Dataset	$\mu$ Bi-ConvLSTM	DeepConvLSTM	TinyHAR	TinierHAR
UCI-HAR	<b>420</b>	16,620	6,050	1,080
MotionSense	<b>389</b>	16,490	4,270	740
WISDM	<b>359</b>	16,370	2,480	402
PAMAP2	<b>523</b>	17,030	12,010	2,210
Opportunity	<b>1,140</b>	19,480	47,770	8,970
UniMiB	<b>359</b>	16,370	2,480	402
SKODA	<b>444</b>	13,290	12,360	1,910
Daphnet	<b>245</b>	8,110	2,640	399
<b>Average</b>	<b>485</b>	15,510	9,290	1,730

Figure 3 reveals that  $\mu$ Bi-ConvLSTM occupies the Pareto-optimal region for the ultra-lightweight regime (top left), achieving competitive accuracy at substantially lower computational cost than all baselines. The separation from TinierHAR demonstrates that further parameter reduction remains viable without catastrophic accuracy loss.

The efficiency heatmap (Figure 4) confirms that  $\mu$ Bi-ConvLSTM parameter efficiency advantage is consistent across all benchmarks rather than dataset specific, indicating a fundamental architectural benefit. Table V details per dataset MACs. Notably, even on 79 channel Opportunity,  $\mu$ Bi-ConvLSTM requires only 1.14M MACs compared to TinyHAR’s 47.8M, a  $42\times$  reduction attributable to avoiding quadratic attention complexity.

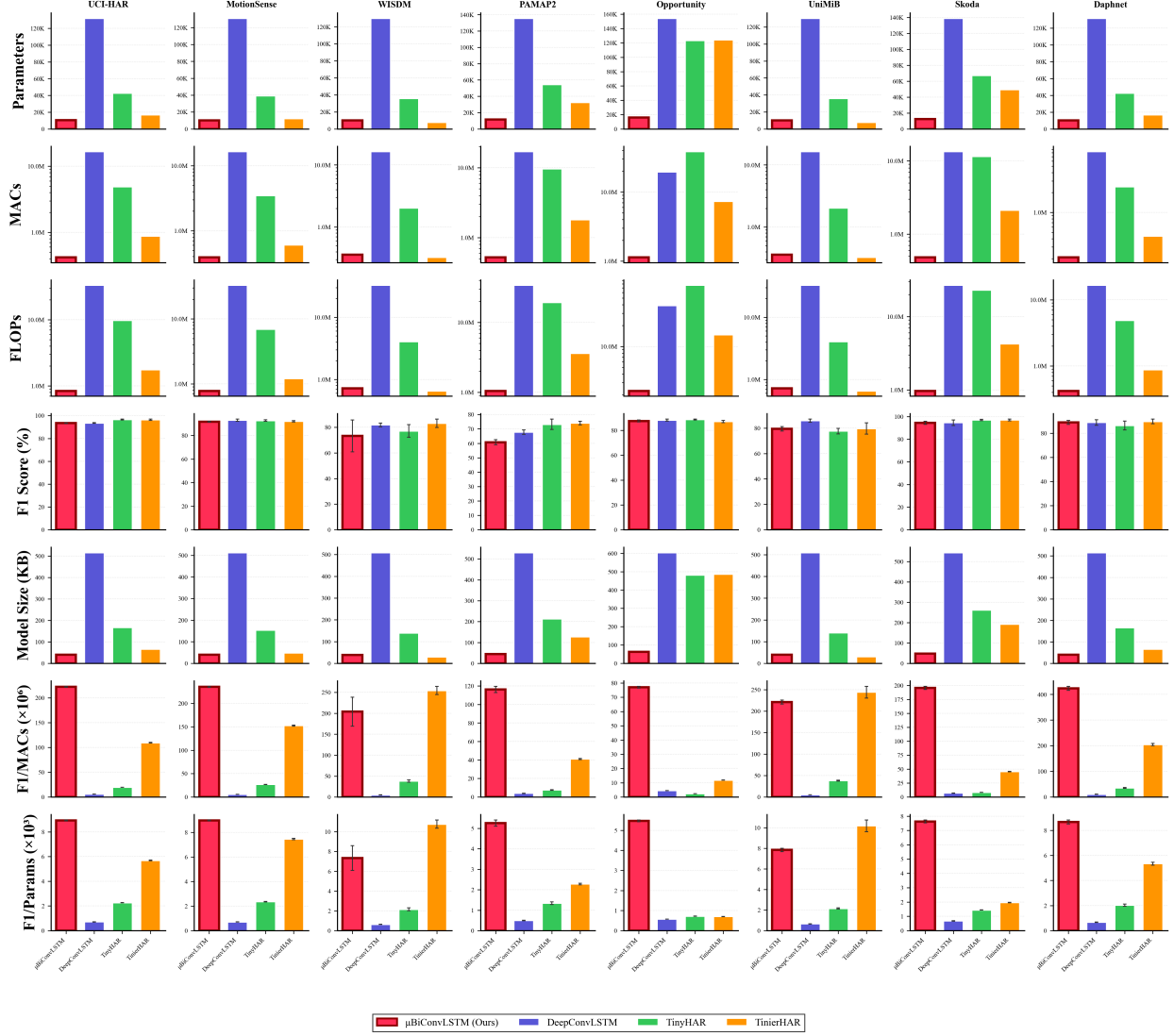
### C. Quantization Analysis

Table VI presents INT8 post training quantization results.  $\mu$ Bi-ConvLSTM shows remarkable quantization robustness with only 0.21% average F1 degradation. Interestingly, PAMAP2 and Opportunity show slight *improvements* after quantization ( $-0.06\%$ ), suggesting that reduced numerical precision provides implicit regularization beneficial for these noisy multi sensor datasets. The Daphnet degradation (1.09%) is acceptable given the binary classification task’s inherent robustness to small prediction shifts.

This quantization resilience likely stems from our architectural simplicity: batch normalization after each convolution constrains activation ranges, the single LSTM layer avoids error accumulation through stacked quantized operations, and the  $4\times$  temporal pooling reduces the number of quantized computations. Figure 5 visualizes this robustness.

### D. Memory Footprint Analysis

Table VII presents INT8 memory requirements across all datasets, with overhead expressed as percentage increase relative to  $\mu$ Bi-ConvLSTM. Our architecture averages 23.0 KB, while TinierHAR requires 66% more memory, TinyHAR requires 385% more, and DeepConvLSTM requires 1,056%

Benchmark Comparison:  $\mu$ BiConvLSTM vs Baselines Across HAR Datasets

**Fig. 2:** Parameters, MACs, FLOPs, Model Size (in KB), F1-score per million MACs, and F1-score per thousand parameters distributions across architectures and datasets. Box plots show mean, and standard deviations across five random seeds.  $\mu$ Bi-ConvLSTM (leftmost in each group) maintains competitive variance despite 2.9 $\times$  fewer parameters than TinierHAR.

TABLE VI: INT8 Quantization Impact on  $\mu$ Bi-ConvLSTM

Dataset	FP32 F1	INT8 F1	Degradation
UCI-HAR	0.9269	0.9269	<b>0.00%</b>
MotionSense	0.9088	0.9046	0.42%
WISDM	0.7684	0.7682	0.02%
PAMAP2	0.6373	0.6379	-0.06%
Opportunity	0.8703	0.8709	-0.06%
SKODA	0.9571	0.9564	0.07%
Daphnet	0.8813	0.8705	1.09%
<b>Average</b>	0.8500	0.8479	<b>0.21%</b>

more. This positions  $\mu$ Bi-ConvLSTM as the architecture consistently viable for memory constrained edge devices across all tested configurations.

TABLE VII: Memory Footprint (INT8, KB) with Overhead vs  $\mu$ Bi-ConvLSTM

Dataset	$\mu$ Bi-ConvLSTM	TinierHAR	TinyHAR	DeepConvLSTM
UCI-HAR	<b>21.2</b>	34.1	84.7	264.3
MotionSense	<b>20.7</b>	33.6	72.2	263.6
WISDM	<b>20.2</b>	33.0	59.7	262.8
PAMAP2	<b>23.4</b>	37.7	124.7	267.8
Opportunity	<b>32.4</b>	56.7	305.0	295.5
UniMiB	<b>20.5</b>	33.3	59.7	263.1
SKODA	<b>25.1</b>	43.1	128.4	256.3
Daphnet	<b>20.8</b>	33.6	58.3	252.6
<b>Average</b>	<b>23.0</b>	38.1	111.6	265.8
Overhead vs $\mu$ Bi-ConvLSTM	—	+66%	+385%	+1,056%

Notably,  $\mu$ Bi-ConvLSTM’s footprint scales gracefully with input dimensionality: the 79 channel Opportunity dataset requires only 32.4 KB (41% increase from the 3 channel

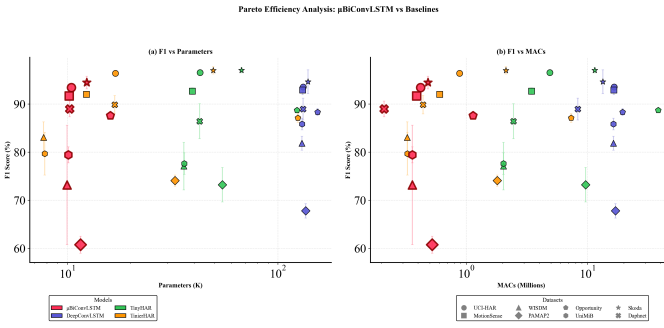


**Fig. 3:** Pareto frontier: F1-score versus MACs (log scale). Each point represents one model-dataset combination.  $\mu$ Bi-ConvLSTM (blue) occupies the top left region, achieving competitive accuracy at lower computational cost.

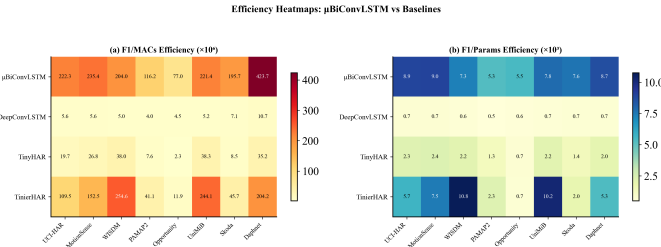


**Fig. 4:** Efficiency heatmap: F1-score per thousand parameters across datasets. Darker cells indicate higher parameter efficiency.  $\mu$ Bi-ConvLSTM advantage is consistent across benchmarks rather than dataset-specific.

minimum), whereas TinyHAR increases to 305 KB (411% increase) due to attention’s quadratic channel scaling. This characteristic makes  $\mu$ Bi-ConvLSTM particularly suitable for multi-sensor wearable platforms where memory budgets are fixed, but sensor configurations may vary.

## VI. ABLATION STUDIES

Systematic ablations were conducted, to validate each architectural component. Five variants are evaluated: A0 (Base), A1 (No Pool) removing max pooling layers, A2 (UniDir) using unidirectional LSTM, A3 (Single Conv) removing the second convolutional stage, and A4 (Mean Pool) replacing last timestep aggregation with mean pooling.

Figure 6 presents ablation results across all variants and datasets. Several insights emerge.

**Task Dependent Bidirectionality:** Removing the backward pass (A2) degrades Daphnet by 4.48%, but *improves* UCI-HAR by 0.83%. This suggests periodic locomotion activities have sufficient forward temporal structure, while episodic events (freezing) benefit from bidirectional context to capture both onset and recovery patterns. However, this benefit is modest compared to other architectural factors.

**Critical Aggregation Choice:** Mean pooling (A4) causes catastrophic 52.43% degradation on UniMiB while minimally affecting WISDM (−0.21%). UniMiB’s fall detection requires identifying brief transient events where the final bidirectional state captures critical endpoint information lost through averaging.

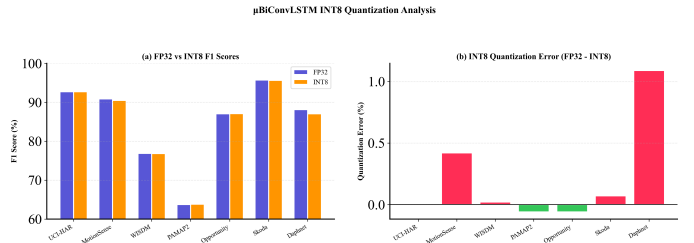


**Fig. 5:** FP32 versus INT8 F1-scores for  $\mu$ Bi-ConvLSTM across datasets. The near diagonal alignment demonstrates quantization robustness, with average degradation of only 0.21%.

**Temporal Compression Value:** Removing max pooling (A1) increases MACs by 3.1 $\times$  with inconsistent accuracy effects, validating the aggressive temporal compression strategy. The pooling layers provide regularization that benefits generalization on smaller datasets.

Hyperparameter sensitivity analysis (varying convFilters 8–24, lstmHidden 16–32) shows the base configuration (16 filters, 24 hidden) sits on the Pareto frontier. Scaling to 24/32 yields only 0.79% average F1 improvement across datasets while nearly doubling parameters (from approximately 10.5K to 19.3K), confirming diminishing returns beyond the base configuration.

## A. Robustness Analysis

Simulating sensor degradation, we find 0.13% F1-score degradation when dropping every 5th sample (jitter), but 86.29% degradation on complete accelerometer dropout, confirming effective sensor specific feature learning rather than trivial signal copying.

Figure 8 provides holistic comparison.  $\mu$ Bi-ConvLSTM achieves strong performance in efficiency dimensions while accepting modest accuracy tradeoffs, demonstrating suitability for deployment scenarios where memory and computational constraints dominate.

## VII. DISCUSSION

### A. Use cases favoring $\mu$ Bi-ConvLSTM

The results reveal that aggressive architectural compression can maintain competitive accuracy when design choices align with task structure:

**Smartphone IMU Data (3-9 channels):** On UCI-HAR and MotionSense,  $\mu$ Bi-ConvLSTM achieves within 3% of larger baselines despite 2.9 $\times$  fewer parameters than TinierHAR. The limited channel count aligns well with our standard convolution design principle (P2).

**Repetitive Industrial Gestures:** SKODA performance (94.46%) demonstrates that 4 $\times$  temporal pooling preserves discriminative features for cyclic assembly tasks where gesture boundaries are well defined.

**Binary Medical Classification:** Competitive Daphnet performance (88.98% vs. TinierHAR’s 89.84%) suggests bidirectional processing captures gait freeze temporal dynamics effectively, though the margin is modest.

Ablation Study: Change ( $\Delta$ ) from Baseline  $\mu$ BiConvLSTM (A0)

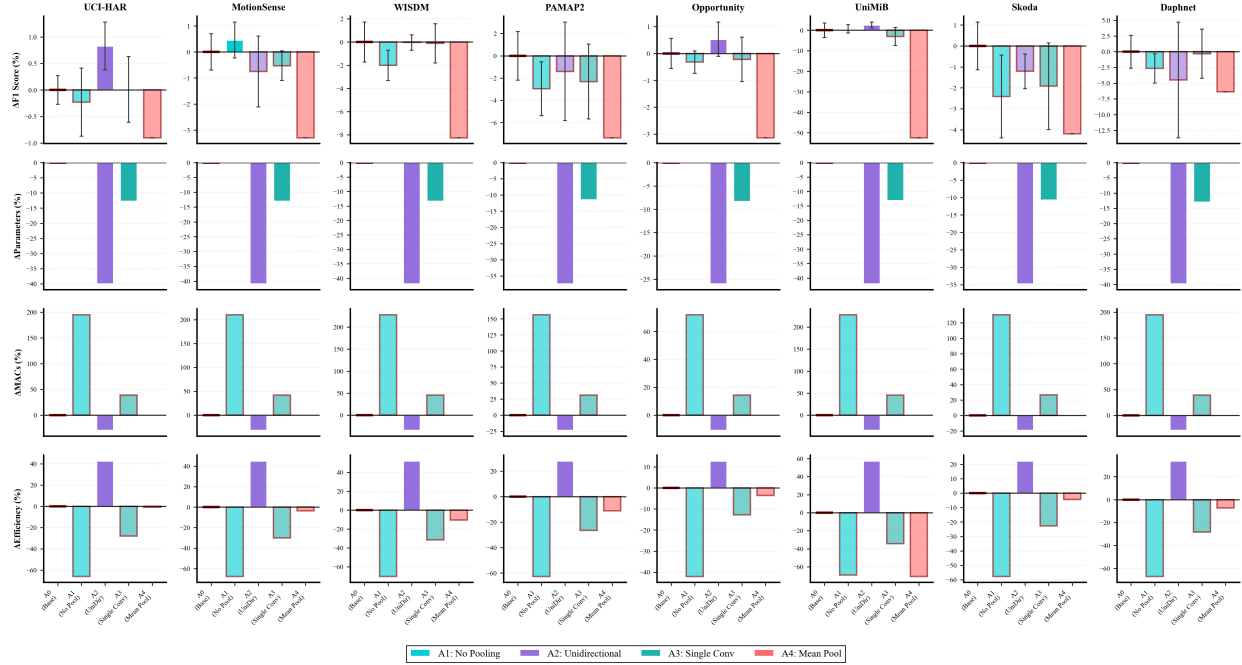


**Fig. 6:** Ablation results across variants (A0–A4) and datasets. A0: Base configuration, A1: No pooling, A2: Unidirectional LSTM, A3: Single conv block, and A4: Mean pooling aggregation.

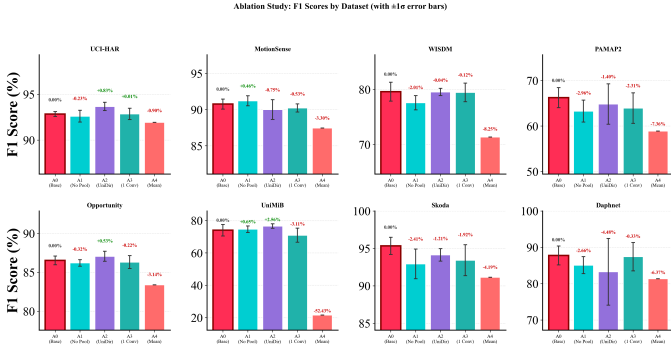


**Fig. 7:** F1-score differences from base configuration (A0) across ablation variants and datasets. The base configuration achieves best or near best performance on 5 of 8 datasets.

## B. Limitations

**Class Imbalance Sensitivity:** On PAMAP2,  $\mu$ BiConvLSTM shows a 13.3% F1-score gap as compared to TinierHAR due to extreme class imbalance where rare activities (rope jumping, cycling) constitute  $<10\%$  of samples, causing ultra-lightweight models to prioritize majority classes under capacity constraints. Notably, Opportunity achieves competitive performance (87.58% vs. 87.09%) despite 79 channels, demonstrating that class distribution impacts ultra-lightweight models more than sensor dimensionality. Practitioners working with severely imbalanced datasets should consider larger architectures or specialized sampling strategies.

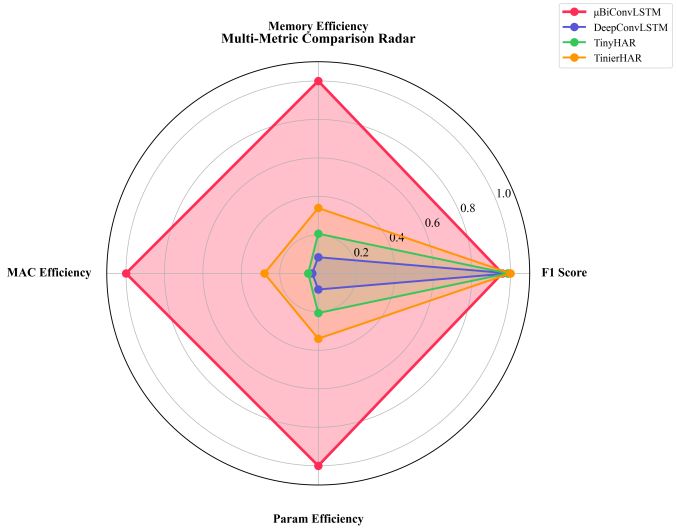


**Fig. 8:** Radar plot comparing four architectures across five normalized metrics: accuracy (mean F1-score), parameter efficiency (F1 per thousand parameters), computational efficiency (F1 per million MACs), memory efficiency (inverse of INT8 model size in KB), and quantization robustness (1 minus degradation percentage). All metrics are scaled to [0,1] where larger values indicate better performance.  $\mu$ Bi-ConvLSTM achieves the largest area in efficiency dimensions while accepting modest accuracy tradeoffs.

**High Variance on Challenging Datasets:** WISDM results show 12.4% standard deviation, likely due to the dataset's lower sampling rate (20 Hz) and minimal channel count

(3) creating challenging learning dynamics. This suggests sensitivity to data quality in the ultra-lightweight regime.

**Modest Bidirectionality Benefits:** Ablation studies reveal bidirectionality provides inconsistent benefits across tasks. For periodic activities like walking, unidirectional processing suffices or even improves performance. The parameter cost of bidirectionality (approximately 50% of LSTM parameters) may not be justified for all applications.

### C. Deployment Considerations

$\mu$ Bi-ConvLSTM’s compact footprint (an average of 23.0 KB INT8) positions it for memory constrained embedded platforms. The architecture’s  $O(N)$  complexity ensures predictable and efficient resource usage across varying sequence lengths, avoiding the quadratic scaling of attention-based alternatives.

The natural deployment strategy:  $\mu$ Bi-ConvLSTM for single sensor wearable applications requiring extreme parameter efficiency, with larger models reserved for multi-sensor configurations where capacity limitations become apparent.

## VIII. CONCLUSION

$\mu$ Bi-ConvLSTM is an ultra-lightweight HAR architecture achieving  $2.9\times$  parameter reduction as compared to Tinier-HAR (11.4K vs. 34K parameters on average) while maintaining competitive accuracy within the ultra-lightweight regime. Key design choices include aggressive  $4\times$  temporal pooling, single layer bidirectional LSTM, and last timestep aggregation, enabling a 23.0 KB INT8 average deployment footprint with only 0.21% quantization degradation.

Our systematic evaluation reveals both strengths and limitations.  $\mu$ Bi-ConvLSTM excels on smartphone IMU datasets (within 3% of larger baselines) and binary medical classification, but shows sensitivity to severe class imbalance on datasets like PAMAP2. Ablation studies demonstrate that architectural contributions are task dependent: bidirectionality benefits episodic event detection, but provides marginal or negative impact on periodic activities.

These findings suggest that the ultra-lightweight regime ( $<15$ K parameters) is viable for single sensor wearable applications, but requires careful task architecture matching. Future work will investigate Neural Architecture Search for sensor modality specific configurations, and knowledge distillation to recover accuracy gaps while preserving the compact footprint.

## REFERENCES

- [1] F. J. Ordóñez and D. Roggen, “Deep convolutional and LSTM recurrent neural networks for multimodal wearable activity recognition,” *Sensors*, vol. 16, no. 1, p. 115, 2016.
- [2] Y. Zhou, H. Zhao, Y. Huang, T. Radu, M. Constantinides, and S. Mehrotra, “TinyHAR: A lightweight deep learning model designed for human activity recognition,” in *Proc. ACM Int. Symp. Wearable Comput.*, 2022, pp. 89–93.
- [3] S. Bian, M. Liu, V. F. Rey, D. Geissler, and P. Lukowicz, “TinierHAR: Towards ultra-lightweight deep learning models for efficient human activity recognition on edge devices,” in *Proc. ACM Int. Joint Conf. Pervasive Ubiquitous Comput.*, 2025.
- [4] Y. Guan and T. Plötz, “Ensembles of deep LSTM learners for activity recognition using wearables,” *Proc. ACM Interact. Mob. Wearable Ubiquitous Technol.*, vol. 1, no. 2, pp. 1–28, 2017.
- [5] N. Y. Hammerla, S. Halloran, and T. Plötz, “Deep, convolutional, and recurrent models for human activity recognition using wearables,” in *Proc. Int. Joint Conf. Artif. Intell.*, 2016, pp. 1533–1540.
- [6] K. Chen, D. Zhang, L. Yao, B. Guo, Z. Yu, and Y. Liu, “Deep learning for sensor-based human activity recognition: Overview, challenges, and opportunities,” *ACM Comput. Surv.*, vol. 54, no. 4, pp. 1–40, 2021.
- [7] D. Ravi, C. Wong, B. Lo, and G.-Z. Yang, “Deep learning for health informatics,” *IEEE J. Biomed. Health Inform.*, vol. 21, no. 1, pp. 4–21, 2017.
- [8] A. Ignatov, “Real-time human activity recognition from accelerometer data using convolutional neural networks,” *Appl. Soft Comput.*, vol. 62, pp. 915–922, 2018.
- [9] A. Bulling, U. Blanke, and B. Schiele, “A tutorial on human activity recognition using body-worn inertial sensors,” *ACM Comput. Surv.*, vol. 46, no. 3, pp. 1–33, 2014.
- [10] J. R. Kwapisz, G. M. Weiss, and S. A. Moore, “Activity recognition using cell phone accelerometers,” *ACM SIGKDD Explor. Newsl.*, vol. 12, no. 2, pp. 74–82, 2011.
- [11] D. Anguita, A. Ghio, L. Oneto, X. Parra, and J. L. Reyes-Ortiz, “A public domain dataset for human activity recognition using smartphones,” in *Proc. Eur. Symp. Artif. Neural Netw.*, 2013, pp. 437–442.
- [12] M. Malekzadeh, R. G. Clegg, A. Cavallaro, and H. Haddadi, “Mobile sensor data anonymization,” in *Proc. ACM/IEEE Int. Conf. Internet Things Design Implement.*, 2019, pp. 49–58.
- [13] R. Chavarriaga, H. Saghaf, A. Calatroni, S. T. Digumarti, G. Tröster, J. d. R. Millán, and D. Roggen, “The Opportunity challenge: A benchmark database for on-body sensor-based activity recognition,” *Pattern Recognit. Lett.*, vol. 34, no. 15, pp. 2033–2042, 2013.
- [14] T. Stiefmeier, D. Roggen, G. Ogris, P. Lukowicz, and G. Tröster, “Wearable activity tracking in car manufacturing,” *IEEE Pervasive Comput.*, vol. 7, no. 2, pp. 42–50, 2008.
- [15] M. Bächlin, M. Plotnik, D. Roggen, I. Maidan, J. M. Hausdorff, N. Giladi, and G. Tröster, “Wearable assistant for Parkinson’s disease patients with the freezing of gait symptom,” *IEEE Trans. Inf. Technol. Biomed.*, vol. 14, no. 2, pp. 436–446, 2010.
- [16] A. Reiss and D. Stricker, “Introducing a new benchmarked dataset for activity monitoring,” in *Proc. Int. Symp. Wearable Comput.*, 2012, pp. 108–109.
- [17] D. Micucci, M. Mobilio, and P. Napoletano, “UniMiB SHAR: A dataset for human activity recognition using acceleration data from smartphones,” *Appl. Sci.*, vol. 7, no. 10, p. 1101, 2017.
- [18] I. Loshchilov and F. Hutter, “Decoupled weight decay regularization,” in *Proc. Int. Conf. Learn. Represent.*, 2019.
- [19] T. Akiba, S. Sano, T. Yanase, T. Ohta, and M. Koyama, “Optuna: A next-generation hyperparameter optimization framework,” in *Proc. ACM SIGKDD Int. Conf. Knowl. Discov. Data Mining*, 2019, pp. 2623–2631.
- [20] S. Hochreiter and J. Schmidhuber, “Long short-term memory,” *Neural Comput.*, vol. 9, no. 8, pp. 1735–1780, 1997.
- [21] A. Graves, A.-r. Mohamed, and G. Hinton, “Speech recognition with deep recurrent neural networks,” in *Proc. IEEE Int. Conf. Acoust. Speech Signal Process.*, 2013, pp. 6645–6649.
- [22] M. Schuster and K. K. Paliwal, “Bidirectional recurrent neural networks,” *IEEE Trans. Signal Process.*, vol. 45, no. 11, pp. 2673–2681, 1997.
- [23] S. Ioffe and C. Szegedy, “Batch normalization: Accelerating deep network training by reducing internal covariate shift,” in *Proc. Int. Conf. Mach. Learn.*, 2015, pp. 448–456.
- [24] N. Srivastava, G. Hinton, A. Krizhevsky, I. Sutskever, and R. Salakhutdinov, “Dropout: A simple way to prevent neural networks from overfitting,” *J. Mach. Learn. Res.*, vol. 15, no. 1, pp. 1929–1958, 2014.
- [25] K. He, X. Zhang, S. Ren, and J. Sun, “Delving deep into rectifiers: Surpassing human-level performance on ImageNet classification,” in *Proc. IEEE Int. Conf. Comput. Vis.*, 2015, pp. 1026–1034.
- [26] D. P. Kingma and J. Ba, “Adam: A method for stochastic optimization,” in *Proc. Int. Conf. Learn. Represent.*, 2015.
- [27] B. Jacob, S. Kligys, B. Chen, M. Zhu, M. Tang, A. Howard, H. Adam, and D. Kalenichenko, “Quantization and training of neural networks for efficient integer-arithmetic-only inference,” in *Proc. IEEE Conf. Comput. Vis. Pattern Recognit.*, 2018, pp. 2704–2713.
- [28] R. Krishnamoorthi, “Quantizing deep convolutional networks for efficient inference,” *arXiv preprint arXiv:1806.08342*, 2018.
- [29] C. R. Banbury, V. J. Reddi, M. Lam, W. Fu, A. Faber, M. Mattina, P. Whatmough, L. Lee, H. Tiber, D. Wijayasinghe, et al., “MLPerf Tiny benchmark,” in *Proc. NeurIPS Datasets Benchmarks Track*, 2021.

- [30] P. Warden and D. Situnayake, *TinyML: Machine Learning with Tensor-Flow Lite on Arduino and Ultra-Low-Power Microcontrollers*. O'Reilly Media, 2019.
- [31] J. Lin, W.-M. Chen, Y. Lin, J. Cohn, C. Gan, and S. Han, “MCUNet: Tiny deep learning on IoT devices,” in *Proc. Adv. Neural Inf. Process. Syst.*, 2020, pp. 11711–11722.
- [32] L. Lai, N. Suda, and V. Chandra, “CMSIS-NN: Efficient neural networks on ARM Cortex-M CPUs,” *arXiv preprint arXiv:1801.06601*, 2018.
- [33] A. Abedin, M. Ehsanpour, Q. Shi, H. Rezatofighi, and D. C. Ranasinghe, “Attend and discriminate: Beyond the state-of-the-art for human activity recognition using wearable sensors.” *Proc. ACM Interact. Mob. Wearable Ubiquitous Technol.*, vol. 5, no. 1, pp. 1–22, 2021.
- [34] S. Liu, S. Yao, J. Li, D. Liu, T. Wang, H. Shao, and T. Abdelzaher, “GlobalFusion: A global attentional deep learning framework for multisensor information fusion,” *Proc. ACM Interact. Mob. Wearable Ubiquitous Technol.*, vol. 4, no. 1, pp. 1–27, 2020.
- [35] H. Ma, W. Li, X. Zhang, S. Gao, and S. Lu, “AttnSense: Multi-level attention mechanism for multimodal human activity recognition,” in *Proc. Int. Joint Conf. Artif. Intell.*, 2019, pp. 3109–3115.
- [36] V. S. Murahari and T. Plötz, “On attention models for human activity recognition,” in *Proc. ACM Int. Symp. Wearable Comput.*, 2018, pp. 100–103.
- [37] Y. Zhou, T. King, H. Zhao, Y. Huang, T. Riedel, and M. Beigl, “MLP-HAR: Boosting performance and efficiency of HAR models on edge devices with purely fully connected layers,” in *Proc. ACM Int. Symp. Wearable Comput.*, 2024, pp. 133–139.
- [38] S. Deng, J. Chen, D. Teng, C. Yang, D. Chen, T. Jia, and H. Wang, “LHAR: Lightweight human activity recognition on knowledge distillation,” *IEEE J. Biomed. Health Inform.*, 2023.
- [39] M.-K. Yi, W.-K. Lee, and S. O. Hwang, “A human activity recognition method based on lightweight feature extraction combined with pruned and quantized CNN for wearable device,” *IEEE Trans. Consum. Electron.*, vol. 69, no. 3, pp. 657–670, 2023.
- [40] W.-S. Lim, W. Seo, D.-W. Kim, and J. Lee, “Efficient human activity recognition using lookup table-based neural architecture search for mobile devices,” *IEEE Access*, vol. 11, pp. 71727–71738, 2023.
- [41] A. Vaswani, N. Shazeer, N. Parmar, J. Uszkoreit, L. Jones, A. N. Gomez, Ł. Kaiser, and I. Polosukhin, “Attention is all you need,” in *Proc. Adv. Neural Inf. Process. Syst.*, 2017, pp. 5998–6008.
- [42] E. Lattanzi, L. Calisti, and C. Contoli, “Are Transformers a useful tool for tiny devices in human activity recognition?,” in *Proc. 8th Int. Conf. Advances Artif. Intell.*, 2024, pp. 339–344.
- [43] M. Bock, A. Hölzemann, M. Moeller, and K. Van Laerhoven, “Improving deep learning for HAR with shallow LSTMs,” in *Proc. Int. Symp. Wearable Comput.*, 2021, pp. 7–12.
- [44] Y. L. Coelho, F. de Assis Souza dos Santos, A. Frizera-Neto, and T. Freire Bastos-Filho, “A lightweight framework for human activity recognition on wearable devices,” *IEEE Sensors J.*, vol. 21, no. 21, pp. 24471–24481, 2021.
- [45] C. A. Ronao and S.-B. Cho, “Human activity recognition with smartphone sensors using deep learning neural networks,” *Expert Syst. Appl.*, vol. 59, pp. 235–244, 2016.